Article

Ir-skinned Ir-Cu Nanoparticles with Enhanced Activity for Oxygen Reduction Reaction

WANG Jiarui[1#], ZHOU Ye[1,2#], SUN Libo[1,2#], GE Jingjie[1], WANG Jingxian[1], DAI Chencheng[1] and XU Zhichuan[1,2,3*]

1. School of Materials Science & Engineering, Nanyang Technological University, 50 Nanyang Avenue 639798, Singapore;

2. Solar Fuels Laboratory, Nanyang Technological University, 50 Nanyang Avenue 639798, Singapore;

3. Energy Research Institute@NTU, ERI@N, Interdisciplinary Graduate School, Nanyang Technological University, 50 Nanyang Avenue 639798, Singapore

Abstract The development of methanol-tolerate oxygen reduction reaction(ORR) electrocatalysts is of special significance to direct methanol fuel cells system. Iridium is known for its better methanol tolerance than platinum and able to survive in harsh acidic environment. However, its activity is relatively low and thus the approach to improve Ir's ORR is desired. Herein, bimetallic Ir-Cu nanoparticles(NPs) with controllable Ir/Cu compositions(*ca.* 1:2 to 4:1, atomic ratio) are synthesized *via* a galvanic replacement-based chemical method. The as-synthesized Ir-Cu NPs are investigated as ORR catalysts after electrochemically leaching out the surface Cu and forming Ir-skinned structures. Around 2- to 3-fold enhancement in the intrinsic activity has been observed in these Ir-skinned Ir-Cu catalysts compared to Ir counterpart. The approach is demonstrated to be a promising way to prepare efficient Ir ORR catalysts and lower catalyst cost.

Keywords Iridium; Copper; Nanoparticle; Dealloying; Oxygen reduction reaction

1 Introduction

Fuel cells are a class of promising energy conversion devices that involve two reactions, the electrochemical oxidation of fuels and reduction of oxygen at the anode and cathode, respectively. The cathodic ORR is a limiting reaction for the overall efficiency of hydrogen proton exchange membrane (PEM) fuel cells due to its slow kinetics[1,2]. While platinum(Pt) is known to be the most effective electrocatalyst for ORR, the poor methanol tolerance hinders its applicability in the direct methanol fuel cell(DMFC) because of the fuel cross-over issue and the dehydrogenation of methanol to adsorbed CO on Pt cathode[3,4]. DMFC is one of the most attractive fuel cells in the next-generation energy systems due to the high energy density and ease-handling of liquid methanol fuel[3]. Thus seeking alternatives to Pt, especially methanol-tolerant oxygen reduction electrocatalysts, is of special significance to the development of DMFC. Among the platinum group metals, iridium(Ir) has been known as a methanol-tolerant catalyst for DMFC[5,6]. Although Ir is more stable in acidic media and more cost-effective, comparing with Pt, its scarcity and comparative low activity for ORR greatly inhibited its wide application in DMFC. Thus, efforts are devoted to improving its activity. Those approaches include morphology controlling to expose specific crystal plane, building nanostructures to exhibit more active sites[2], modulating electronic state *via* doping or synthesizing multi-metal alloys or compounds[7,8]. Among all these methods, controllable synthesis of Ir-based nanoalloys appears to be more attractive. Because it can not only modulate electronic state of active sites, but also increase the effectiveness of Ir by partially reducing the internal inert consumption of Ir. Up to now, a series of Ir nanoalloys, including Ir-based nanoframes[9], nanocages[10], and octahedral structures[11], has been reported to exhibit much better than its counterpart. However, the investigation on Ir-based nanoalloys, or its derivative towards ORR in acidic media is very limited. On the other hand, Cu has been widely used as alloying metal in electrocatalysis system due to its easy synthesis and controllable dealloying property. In this paper, we finely controlled the composition of Ir-Cu nanoparticles *via* a facile chemical reduction method and electrochemical post-leaching procedures and elaborately studied their influence on the ORR performance. Specifically, Ir-Cu bimetallic NPs with atomic ratios of Cu to Ir varying from *ca.*1:2 to 4:1 were synthesized and used as ORR catalysts after electrochemically leaching out the surface Cu to form Ir-skin structures. The Ir-skinned catalysts showed excellent electrocatalytic ORR activity compared with that of Ir NPs in acidic media. The improved activity is ascribed to both the

*Corresponding author. Email: xuzc@ntu.edu.sg

#These authors contributed equally to this work.

Received March 31, 2020; accepted May 5, 2020.

Supported by the Project of the Singapore Ministry of Education Tier 2(No.MOE2017-T2-1-009) and the Singapore National Research Foundation Under Its Campus for Research Excellence and Technological Enterprise(CREATE) Programme.

increase of active surface area *via* Cu dealloying and enhanced electronic structures. This facile chemical reduction and post dealloying method is promising for synthesizing other prominent metal-metal nanoalloy catalysts.

2 Experimental

2.1 Materials

Iridium(III) acetylacetonate[$Ir(acac)_3$, 99%], Cu(II) acetylacetonate[$Cu(acac)_2$, 99.9%], and oleylamine($C_{18}H_{35}NH_2$, 70%) were purchased from Aldrich. Vulcan carbon(Vulcan XC-72) was purchased from FuelCellStore Co. All chemicals were used without further purification.

2.2 Synthesis of Catalysts

Ir-Cu binary metallic catalysts with atomic ratios of Cu to Ir varying from *ca*. 1:2 to 4:1 were prepared *via* a thermal decomposition method under Ar atmosphere. Briefly, 1 mmol of $Ir(acac)_3$ and $Cu(acac)_2$ in total were added to a three-neck flask with oleylamine(8 mL). The feeding ratios of $Cu(acac)_2$ to $Ir(acac)_3$ were 1:2, 1:1, 2:1 and 3:1, respectively. With constant stirring, the mixture solution was dehydrated at 110 ℃ for 1 h and heated to 240 ℃ at a heating rate of 8 ℃/min. After aging at 240 ℃ for 1 h and cooling down, the products were precipitated by adding ethanol and hexane. The collected nanoparticles by centrifugation(10000 r/min, 15 min) were dispersed in hexane. To avoid aggregation, the Ir-Cu nanoparticles were further loaded onto a Vulcan carbon(Vulcan XC-72). Vulcan carbon(100 mg) was first dispersed in 100 mL of hexane through ultra-sonication for 2 h. Then, the as-synthesized nanoparticles dispersion was added dropwise into the solution. The mixture was kept sonicating for another 1 h in ice bath and stirring overnight. The final Vulcan carbon supported NPs catalysts were separated and collected by centrifugation. To prepare the working electrodes, the catalysts(catalyst concentration: 5 mg/mL) were dispersed in a mixture of ethanol(0.985 mL) and Nafion solution(5%, mass fraction, 0.015 mL) by sonication for at least 30 min to form a homogeneous ink. Then 7.5 μL of catalyst ink was cast on the newly polished glassy carbon electrode and dried under an ambient condition[mass loading: 38.3 μg(Ir-Cu NPs)/cm^2_{disk}]. The electrochemical measurements were carried out in 0.1 mol/L $HClO_4$ electrolyte with platinum wire and Ag/AgCl as counter and reference electrodes, respectively. The catalysts were first subject to cyclic voltammetry(CV) scans from 0 to 0.85 V *vs*. RHE at 100 mV/s in Ar-saturated 0.1 mol/L $HClO_4$ electrolyte until stable CV curves were obtained. Then the ORR CV curves were recorded at a scan rate of 10 mV/s in a new batch of O_2 saturated 0.1 mol/L $HClO_4$ with rotating speeds varying from 100 r/min to 2500 r/min(100, 400, 900, 1600, and 2500 r/min).

2.3 Material Characterization

The powder X-ray diffraction(XRD) measurements were recorded using a Bruker D8 Advance X-ray diffractometer (Cu *Kα* radiation, λ=0.154 nm), and the diffractometer operating conditions were 40 kV, and 30 mA. The scanning electron microscopy-energy dispersive X-ray spectroscopy(SEM-EDX) mapping(to determine the atomic ratios of Ir/Cu) was recorded on a 7600F field-emission scanning electron microscope (FESEM) operating at 15 kV. At least 6 different positions were probed to obtain an average value of atomic ratios. The transmission electron microscopy(TEM) and high resolution electron microscopy(HRTEM) characterization and size analysis on nanoparticles were performed on a JEOL 2100F transmission electron microscope at 200 kV. The average diameter d_n, the volume/area averaged diameter $d_{v/a}$ and the surface area of the nanoparticles[12] were calculated as follows:

$$d_n = \frac{\sum_{i=1}^{n} d_i}{n} \tag{1}$$

$$d_{v/a} = \frac{\sum_{i=1}^{n} d_i^3}{\sum_{i=1}^{n} d_i^2} \tag{2}$$

$$S_v = \frac{6000}{\rho \cdot d_{v/a}} \tag{3}$$

where d is the diameter of individual nanoparticle, n is the number of counted nanoparticles. S_v is the specific surface area in m^2/g Ir-Cu, ρ is the theoretic density of Ir-Cu alloy. X-Ray photoelectron spectroscopy(XPS) measurements were performed on a Kratos AXIS Supra with an automated dual anode (Al *Kα*) X-ray monochromatic source.

3 Results and Discussion

Monodispersed Ir-Cu NPs with atomic ratios of Cu to Ir varying from *ca*. 1:2 to 4:1 were prepared by a facile thermal decomposition method. Briefly, 1 mmol of $Ir(acac)_3$ and $Cu(acac)_2$ in total were added to a three-neck flask with oleylamine(8 mL). The feeding ratios of $Cu(acac)_2$ to $Ir(acac)_3$ were 1:2, 1:1, 2:1 and 3:1, respectively. With constant stirring, the mixture solution was dehydrated at 110 ℃ for 1 h and heated to 240 ℃ at a heating rate of 8 ℃/min. After aging at 240 ℃ for 1 h and cooling down, the products were precipitated by adding ethanol and hexane. Insights into the formation of Ir-Cu alloy were revealed by tracking the UV-Vis absorption spectra of the intermediate products at different reaction stages. As shown in Fig.1(A), the appearance of peaks at *ca.* 256 and 304 nm indicates the preliminary reduction of Cu^{2+} to Cu NPs at 180 ℃[13]. As the reaction temperature approaches 240 ℃, absorption peaks at *ca*. 261 and 284 nm emerged. These distinct peaks can be ascribed to the characteristic absorption of Cu NPs according to Mie theory(dipole oscillation)[14]. In contrast, the absence of any significant characteristic surface plasmon absorption, which is usually observed at *ca*. 600 nm for Cu, is mainly due to the small particle size[14,15]. With the reaction proceeds(aging at 240 ℃ for 60 min), Cu NPs peaks(at *ca.* 261 and 284 nm) intensity decreased. The pre-deposited Cu nanoparticles, at this stage, might act as template or reducing source to facilitate the galvanic replacement reaction of $3Cu^0 + 2Ir^{3+} \longrightarrow 3Cu^{2+} + 2Ir^0$[10], leading to the gradual replacement of Cu by Ir. The formation of Ir is also evidenced by the appearance of similar absorption characteristics reported for Ir particles[16]. As known, Ir NPs are difficult to be reduced from

$Ir(acac)_3$ precursor, which needs high temperature up to 300 ℃. In contrast, our thermo- chemical reduction method *via* self-sacrificing the *in-situ* formed Cu NPs template greatly reduced the required temperature.

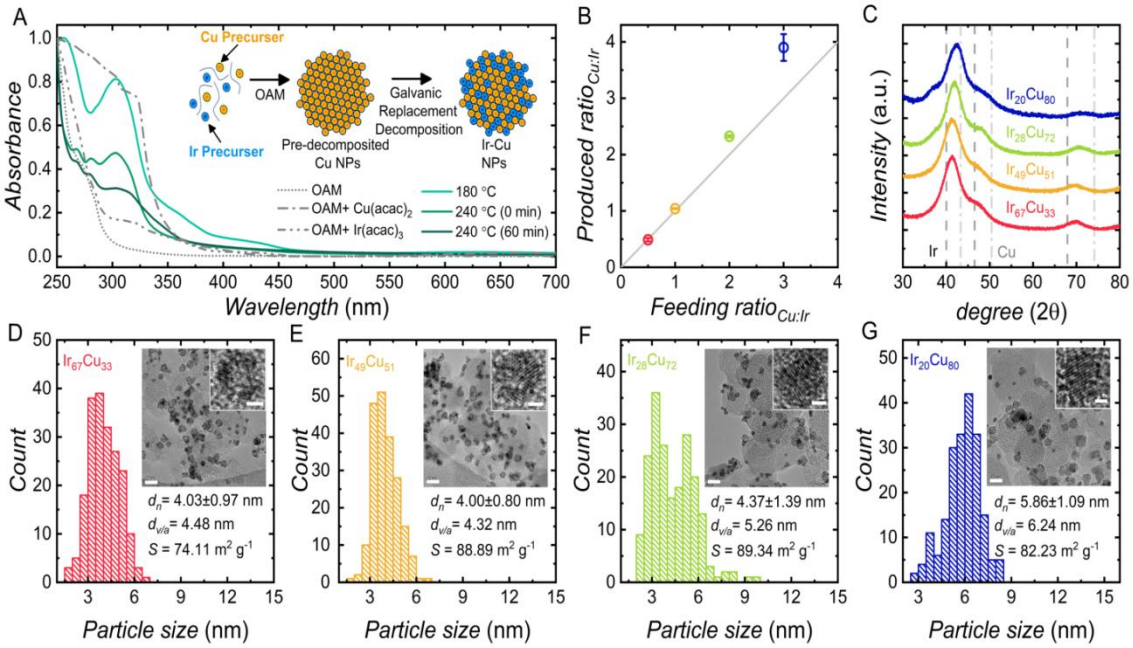

Fig.1 UV-visible spectra of the metal precursors/oleylamine and intermediates at different reaction stages(A), feeding and produced Ir/Cu ratios for Ir-Cu NPs(gray line represents the theoretical product ratio) with the obtained Ir/Cu ratio determined by EDX-SEM)(B), XRD patterns of the as-synthesized Ir-Cu NPs(C) and size distribution of the $Ir_{67}Cu_{33}$(D), $Ir_{49}Cu_{51}$(E) , $Ir_{28}Cu_{72}$(F) and $I_{20}Cu_{80}$ NPs(G)

Inset of (A): schematic synthesis of Ir-Cu nanoparticles(NPs) *via* a thermal decomposition method; insets of (D—G): TEM and HRTEM images of the as-obtained Ir-Cu NPs, the scales are 10 nm and 1 nm respectively..

In order to correlate the feeding ratios with the real ratios in Ir-Cu nanoparticles, EDX analysis was performed to examine the produced Ir/Cu atomic ratios in various Ir-Cu NPs. As shown in Fig.1(B), the initial feeding ratios of Cu to Ir are different from those detected by the EDX. Specifically, the initial feeding ratios(Cu:Ir) of 1:2, 1:1, 2:1 and 3:1 yield ratios of 1:2.04, 1:0.96, 2:0.86 and 3:0.77, respectively. Thus, according to the actual atomic ratios, the as-synthesized Ir-Cu NPs are denoted as $Ir_{67}Cu_{33}$, $Ir_{49}Cu_{51}$, $Ir_{28}Cu_{72}$ and $Ir_{20}Cu_{80}$. The XRD patterns[Fig.1(C)] indicate a face-centered cubic(fcc) structure of the all as-synthesized Ir-Cu NPs, with peak positions located between those of Ir and Cu. A gradual peak shift to higher angles was observed with the increase of Cu concentration. This is due to the lattice contraction caused by the incorporation of smaller Cu into the Ir fcc structure[17]. Cu ions were preferred to be reduced to nanocrystals and the subsequent galvanic replacement of Cu nanostructures with Ir species occurred.

Representative TEM images and the particle size distribution of $Ir_{67}Cu_{33}$, $Ir_{49}Cu_{51}$, $Ir_{28}Cu_{72}$ and $Ir_{20}Cu_{80}$ NPs are shown in Fig.1(D—G). As can be seen, those Ir-Cu NPs display an interior and are well dispersed on the surface of the Vulcan XC-72 support. By counting at least 200 nanoparticles, the average diameter(d_n) and volume/area averaged diameter ($d_{v/a}$) of Ir-Cu NPs were determined. A gradual growth in particle size from *ca.* 4 nm to 6 nm can be detected with increasing Ir/Cu atomic ratio. The surface areas of Ir-Cu NPs were calculated accordingly by using the volume/area averaged diameter ($d_{v/a}$) as it better represents the specific surface area of metal NPs[12].

Therefore, we proposed following mechanism[shown in inset of Fig.1(A)]: the Cu NPs are first formed at a relatively lower temperature through the decomposition of $Cu(acac)_2$ in oleylamine. Then, the pre-deposited Cu NPs serve as template and reducing source of Ir, during which Cu NPs are transformed into Ir-Cu nanoalloys *via* galvanic replacement. The corresponding reaction equation is shown below in Eq.(4).

$$3Cu^0 + 2Ir^{3+} \longrightarrow 3Cu^{2+} + 2Ir^0 \quad (4)$$

In the galvanic replacement reaction, Ir^{3+} is preferentially reduced to metallic Ir in react with Cu^0. In the meantime, the dissolved Cu^{2+} ions can be reduced back to Cu^0 by the oleylamine and combine with metallic Ir to form Ir-Cu alloy. It is worth noticing that, based on the galvanic replacement mechanism[18], the elemental Ir is likely to be confined to the vicinity of the Cu template surface and ultimately evolve into a shell-like structure. At the same time, the continuous diffusion of Ir^{3+} and Cu^{2+} across the initial open shell gradually depletes the Cu template core. This is typically what can be observed for galvanic replacement involved NP formation[18].

The various Ir-Cu NPs were investigated as ORR catalysts in 0.1 mol/L $HClO_4$ after electrochemically leaching out the surface Cu and forming Ir-skin structures. The catalyst inks were prepared by dispersing 5 mg of carbon loaded Ir-Cu particles into 1 mL of ethanol through sonication. The homogeneous ink was then pipetted onto newly polished rotating disk electrode(RDE) to yield a mass loading of *ca.* 38.3 μg(Ir+Cu)/ cm^2_{disk}. The Ir-Cu catalysts were first cycled within a potential window of 0—0.85 V(*vs.* RHE) in

Ar-saturated 0.1 mol/L $HClO_4$ electrolyte solution to remove the surface Cu. As a representative example, Fig.2(A) displays the voltammetry characteristics of $Ir_{20}Cu_{80}$ at different stages of the dealloying process. The first dealloying cycle shows no hydrogen adsorption/desorption features, which might be due to the surface impurities and much Cu coverage. In the second cycle, the dissolution peak of Cu to Cu^{2+} appears at round 0.35 V during the anodic potential sweep. The Cu dissolution peak gets more predominant until the 7th cycle, after which the dissolution peaks decrease in intensity, indicating the gradual removal of Cu. At the same time, the hydrogen adsorption/desorption features(0.05 V to 0.3 V *vs.* RHE) emerge as Ir is increasingly exposed to the surface. The absence of Cu features at the end of the dealloying process suggests the initial $Ir_{20}Cu_{80}$ changed into dealloyed Ir-Cu alloy with an Ir-rich surface. The ORR of dealloyed Ir-skinned catalysts was then performed in a new batch O_2-saturated 0.1 mol/L $HClO_4$ within a potential range of 0.05—1.0 V *vs.* RHE(Fig.S1, see the Electronic Supplementary Material of this paper). The representative ORR polarization curves at different rotating speeds (100, 400, 900, 1600 and 2500 r/min) are shown in Fig.2(B). The diffusion limits are comparable to the values reported for Ir-based catalysts[5]. To determine the effective Ir surface area, CV curves were recorded in Ar-saturated electrolyte after the ORR tests[Fig.2(C)]. The inset of Fig.2(C) shows the obtained Ir surface areas of dealloyed Ir-skins with different metal ratios. The active surface area of Ir decreases with increasing Ir/Cu feeding ratios. Since electrocatalytic reactions only involve the surface atoms, the intrinsic activity of Ir is best reflected by the so-called "specific activity" where activities are normalized by the electroactive surface area of Ir. Fig.2(D) shows the specific activities of the dealloyed Ir-skinned catalysts[ORR current densities were normalized by the Ir electrochemistry surface area(ECSA)] after mass-transport and *iR*(*i* is the current, *R* is the resistance) corrections[19—21]. To evaluate the mass efficiency of Ir in the bulk Ir-Cu NPs, the mass activities of Ir are provided accordingly in Fig.2(E). Both the specific and mass activities of dealloyed Ir-Cu nanoparticles increase in the sequence of $Ir_{67}Cu_{33}$, $Ir_{50}Cu_{50}$, $Ir_{20}Cu_{80}$, and $Ir_{28}Cu_{72}$. The specific and mass activities of dealloyed Ir-skin catalysts were further plotted as current densities at a fixed potential of 0.80 V *vs.* RHE[Fig.2(F)]. It is apparent that catalyst $Ir_{28}Cu_{72}$ exhibits the highest specific and mass activity among all the compositions. For comparison purpose, pure Ir NPs were synthesized *via* a wet chemical method[22] and investigated as catalyst for ORR(Figs.S2 and S3, see the Electronic Supplementary Material of this paper). Compared with pure Ir catalyst[Fig.2(F)], the dealloyed Ir-Cu catalysts exhibit an enhancement of

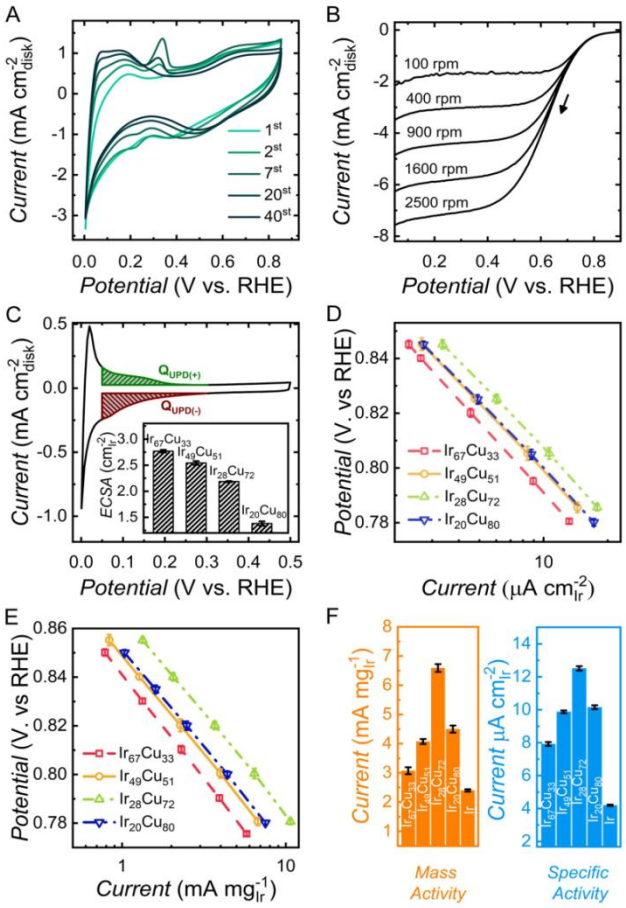

Fig.2 Electrochemical measurements

(A) Dealloying CV cycling of $Ir_{20}Cu_{80}$ NPs in 0.1 mol/L $HClO_4$ at a scan rate of 100 mV/s; (B) representative ORR polarization curves at different rotating speeds; (C) CV curves scanned in 0.1 mol/L $HClO_4$ at a scan rate of 10 mV/s; inset of (C) is the ECSA of Ir in various Ir-Cu catalysts determined from an integration method; (D) Tafel plots based on Ir surface area; (E) Tafel plots based on Ir mass; (F) kinetic current densities(specific and mass current density) at a fixed potential of 0.80 V(*vs.* RHE).

ca.1.3—2.8 and *ca*. 2—3 folds in mass and specific activities, respectively. The multifold increase in intrinsic ORR activity can be attributed to the electronic modification of Ir-skin by the Ir-Cu alloy of different compositions beneath the outermost shell[23]. In the bimetallic Ir-Cu system, it is very likely that the strain and ligand effects act in a cumulative manner and modify the d band structure(d band center, d-band width) of the surface Ir atom[24,25], resulting in the distinctive ORR activities. The importance of these modified d-band structures of Ir can be rationalized by the effective interaction between the surface metal d orbital and the adsorbate orbitals during catalytic ORR[24,25].

To further investigate the methanol-tolerance of the Ir-Cu NPs, the methanol oxidation reaction(MOR) and methanol interference on ORR were investigated. Fig.3(A) shows the cyclic voltammograms of dealloyed $Ir_{28}Cu_{72}$ NPs in argon-saturated $HClO_4$(0.1 mol/L) with and without 1 mol/L methanol at 50 mV/s. No significant current difference can be seen after adding methanol, which shows no obvious methanol oxidation occurred. This indicates that there is no dehydrogenation of methanol on Ir, different from Pt[26,27]. The chronoamperometric methanol interference was compared between dealloyed $Ir_{28}Cu_{72}$ NPs and Pt/C at 0.6 V *vs*. RHE with a rotation speed of 1600 r/min by injecting 1 mL of methanol into 75 mL of O_2-saturated 0.1 mol/L $HClO_4$ electrolyte, which is shown in Fig.3(B). Compared with Pt/C, the Ir-Cu NPs exhibit superior immunity towards methanol interference. After injecting the methanol, the $Ir_{28}Cu_{72}$ NPs remained over 97% of initial activity, while Pt/C dropped severely after adding methanol[2]. It is known that the methanol interference on Pt is due to the dehydrogenation of methanol to adsorbed CO[26,27]. At 0.6 V *vs*. RHE, Pt is unable to generate enough OH on the surface for removing the adsorbed CO. For Ir-Cu, since there is no dehydrogenation of methanol, which is indicated by the in-active methanol oxidation[Fig.3(A)], there is no CO generated and thus the ORR was not interfered by the addition of methanol.

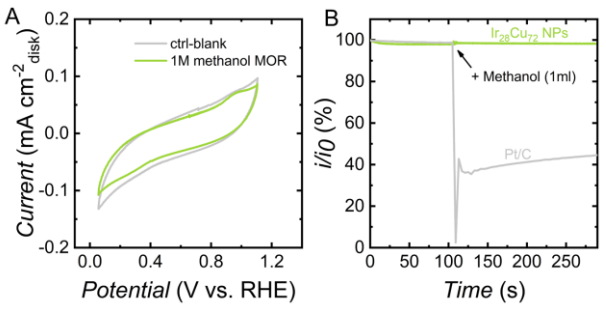

Fig.3 Methanol oxidation of $Ir_{28}Cu_{72}$ NPs(A) and methanol injection of $Ir_{28}Cu_{72}$ NPs and Pt/C(B)

To further confirm our postulation that the striking increase in intrinsic ORR activity is attributed to the electronic modification of Ir-skin by the Ir-Cu alloy of different compositions beneath the outermost shell, X-ray photoelectron spectra (XPS, Fig.4) were recorded for more information of electronic structure. Fig.4(B) and (C) show the Ir_{4f} and Cu_{2p} spectra of $Ir_{28}Cu_{72}$ NPs, respectively, as obtained and after dealloying process. The peaks located at around 61, 61.5, 63.5, 64.4, 932.4, and 933.7 eV could be assigned to $Ir(0)_{4f_{7/2}}$, $Ir^{4+}_{4f_{7/2}}$, $Ir(0)_{4f_{5/2}}$, $Ir^{4+}_{4f_{5/2}}$, $Cu(0)_{2p_{3/2}}$, and $Cu^{2+}_{2p_{3/2}}$, respectively[9]. That indicates the metallic nature of the Ir-Cu nanoparticles. The multifold increase in intrinsic ORR activity can be attributed to the electronic modification of Ir-Cu skin by the Ir-Cu alloy of different compositions beneath the outermost shell. By introducing Cu into Ir, the strain and ligand effect act in a cumulative manner and modify the Ir_{5d} band structure of the surface Ir atom, which is confirmed by the obvious $Ir_{4f_{5/2}}$ orbital negative shift(*ca*. 1 eV) for $Ir_{49}Cu_{51}$ compared with $Ir_{67}Cu_{33}$. It indicates the shell Ir atoms have accepted a partial charge from Cu, which lowers the d-band position as well as the surface oxygen affinity. As shown in Fig.4(B), compared with the as-synthesized $Ir_{28}Cu_{72}$ NPs, the dealloyed one shows an obvious positive shift(0.4 eV) and reduction in Ir^{4+} content, which also suggests a modification of the electronic structure of surface Ir atoms. The importance of these modified d-band structures of Ir can be rationalized by the effective interaction between the surface metal d orbital and the adsorbate orbitals during ORR[28]. Moreover, compared to standard $Ir(0)_{4f_{5/2}}$(binding energy at 60.9 eV[29]), a small negative shift in the binding energy of Cu rich samples $Ir_{49}Cu_{51}$, $Ir_{28}Cu_{72}$ and $Ir_{20}Cu_{80}$ can be observed. This suggests an electronic modification of the near surface Pt atoms by the inner Cu core. Additionally, the reduced $Cu^{2+}_{2p_{3/2}}$ shown in Fig.4(C) indicates weaker oxidation of Cu core of cycled $Ir_{28}Cu_{72}$ NPs. In other words, the formed Ir-skin after de- alloying is protecting inner Cu atoms from oxidation/leaching in(aqueous) perchloric acid. In addition, the reduced specific activity of $Ir_{20}Cu_{80}$ is believed to result from the superfluous oxidation of Ir. The results in Fig.4(A) shows Ir_{4f} changed significantly, the significant rise of Ir^{4+} shows the higher percentage of IrO_x. Ir-oxidation of Ir-skin in Ir-Cu nanoparticles is considerably enhanced under high Cu ratios.

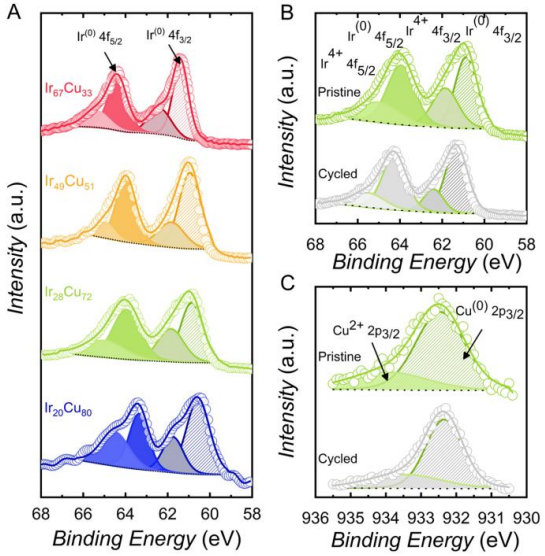

Fig.4 Representative high-resolution XPS spectra of Ir_{4f} of the obtained Ir-Cu NP(A)s and Ir_{4f}(B) and Cu_{2p} of pristine and cycled $Ir_{28}Cu_{72}$ NPs(C)

4 Conclusions

In this work, Ir-Cu NPs with different Cu/Ir ratios were synthesized by a wet-chemical approach. Followed by dealloying in acidic electrolyte, the surface of the nanoparticles became Ir-rich. These dealloyed Ir-skinned catalysts were found to be highly active for ORR with an enhancement of *ca*. 2- to 3-fold in specific activity as compared with the Ir NPs. The enhanced ORR activity was resulted from the optimized electronic structure regulated by the subsurface Ir-Cu layer beneath the Ir-rich surface. By this approach, the usage of Ir for ORR application can be remarkably reduced.

Acknowledgments

The authors acknowledge Facility for analysis, characterication, testing and simulation(FACTS) in Nanyang Technological University for materials characterization.

Electronic Supplementary Material

Supplementary material is available in the online version of this article at http://dx.doi.org/10.1007/s40242-020-0087-1.

References

[1] Zhou Y., Xi S. B., Wang J. X., Sun S. N., Wei C., Feng Z. X., Du Y. H., Xu Z. J., *ACS Catalysis*, **2018**, *8*(1), 673

[2] Wei C., Yu L.H., Cui C.L., Lin J.D., Wei C., Mathews N., Huo F. W., Sritharan T., Xu Z. C., *Chemical Communications*, **2014**, *50*(58), 7885

[3] Lee K., Savadogo O., Ishihara A., Mitsushima S., Kamiya N., Ota Ken-ichiro, *Journal of the Electrochemical Society*, **2006**, *153*(1), A20

[4] Wei C., Rao R. R., Peng J., Huang B., Stephens I. E. L., Risch M., Xu Z. J., Yang S. H., *Advanced Materials*, **2019**, *31*(31), 1806296

[5] Lee K., Zhang L., Zhang J., *Journal of Power Sources*, **2007**, *170*(2), 291

[6] Lee K., Zhang L., Zhang J., *Journal of Power Sources*, **2007**, *165*(1), 108

[7] Zhou Y., Sun S., Xi S., Duan Y., Sritharan T., Du Y., Xu Z. J., *Advanced Materials*, **2018**, *30*(11),1705407

[8] Wu T., Sun S., Song J., Xi S., Du Y., Chen B., Sasangka W. A., Liao H., Gan C. L., Scherer G. G., Zeng L., Wang H., Li H., Grimaud A., Xu Z. J., *Nature Catalysis*, **2019**, *2*(9),763

[9] Pei J., Mao J., Liang X., Chen C., Peng Q., Wang D., Li Y., *Chemical Communications*, **2016**, *52*(19), 3793

[10] Wang C., Sui Y., Xiao G., Yang X, Wei Y, Zou G., Zou B., *Journal of Materials Chemistry A*, **2015**, *3*(39), 19669

[11] Kwon T., Hwang H., Sa Y. J., Park J., Baik H., Joo S. H., Lee K., *Advanced Functional Materials*, **2017**, *27*(7), 1604688

[12] Ferreira P. J., la O' G. J., Yang S. H., Morgan D., Makharia R., Kocha S., Gasteiger H. A., *Journal of The Electrochemical Society*, **2005**, *152*(11), A2256

[13] Ghodselahi T., Vesaghi M., Shafiekhani A., *J. Phys. D: Appl. Phys.*, **2008**, *42*(1), 015308

[14] Díaz-Visurraga J., Daza C., Pozo C., Becerra A., von Plessing C., García A., *International Journal of Nanomedicine*, **2012**, *7*, 3597

[15] Brege J. J., Hamilton C. E., Crouse C. A., Barron A. R., *Nano Lett.*, **2009**, *9*(6), 2239

[16] Chakrapani K., Sampath S., *Chemical Communications*, **2014**, *50*(23), 3061

[17] Toda T., Igarashi H., Uchida H., Watanabe M., *Journal of The Electrochemical Society*, **1999**, *146*(10), 3750

[18] Sun Y., Mayers B., Xia Y., *Adv. Mater.*, **2003**, *15*(7/8), 641

[19] Wei C., Feng Z., Scherer G. G., Barer J., Yang S. H., Xu Z., *Adv. Mater.*, **2017**, *29*, 1606800

[20] Wei C., Sun S., Mandler D., Wang X., Qiao S. Z., Xu Z. J., *Chemical Society Reviews*, **2019**, *48*(9), 2518

[21] Sun S., Li H., Xu Z. J., *Joule*, **2018**, *2*(6), 1024

[22] Nguyen T. D., Scherer G. G., Xu Z. J., *Electrocatalysis*, **2016**, *7*(5), 420

[23] Stamenkovic V. R., Fowler B., Mun B. S., Wang G. F., Ross P. N., Lucas C. A., Markovic N. M., *Science*, **2007**, *315*(5811), 493

[24] Kitchin J. R., Nørskov J. K., Barteau M. A., Chen J. G., *The Journal of Chemical Physics*, **2004**, *120*(21), 10240

[25] Kitchin J. R., Nørskov J. K., Barteau M. A., Chen J. G., *Phys. Rev. Lett.*, **2004**, *93*(15), 156801

[26] Xu Z., Carlton C. E., Allard L. F., Yang S. H., Kimberly H. S., *The Journal of Physical Chemistry Letters*, **2010**, *1*(17), 2514

[27] Suntivich J., Xu Z., Carlton C. E., Kim J., Han B., Lee S. W., Bonnet N., Marzari N., Allard L. F., Gasteiger H. A., Kimberly H. S., Yang S. H., *Journal of the American Chemical Society*, **2013**, *135*(21), 7985

[28] Liu H., Yang J., *Journal of Materials Chemistry A*, **2014**, *2*(19), 7075

[29] Marinova T. S., Kostov K. L., *Surface Science*, **1987**, *181*(3), 573